DEVELOPMENT OF LASER MICRO-ENGRAVING OF PHOTOMASKS

Laser micro-engraving technology is finding more industrial applications, especially in the electronic industry. The lasers used in this technology are mainly Nd:YAG lasers (including fundamental and second harmonic wavelengths), argon ion lasers, and excimer lasers. Two of them, Nd:YAG laser and excimer laser, will be used in our studies. The focal spot diameters at various locations from the laser resonator to the workpiece surface are calculated. The spot size is a key parameter to determine the engraving linewidth. Finally, experiments are performed using both laser machining systems. The experimental results are analysed and compared. It is shown that the use of an excimer laser in the engraving of photomasks produces better results than the use of a Nd:YAG laser.

6.1 Introduction

A photomask consists of a patterned opaque film on a transparent substrate, namely, coating on a mask blank. The quality requirements for mask blanks are: suitable optical transmission, low thermal expansion, low defect levels, and good chemical and mechanical resistance. The characteristics of some common types of glass substrates used in the commercial market are shown in Table 6.1 [6.1, 6.2].

Table 6.1 Characteristics of common types of glass substrate used in photomasks

Property	Feature	Soda lime	White crown	Boro-silicate	Quartz
Thermal	Expansion coefficient, 10^{-7}/°C	94	93	37	5
	Transformation temperature, °C	542	533	686	1120
Optical	Refractive index	1.52	1.52	1.53	1.46
	Specific gravity	2.50	2.56	2.58	2.20
	Young's modulus, kgf/mm^2	7000	7341	7540	7413
Mechanical	Poisson ratio	0.22	0.23	0.16	0.18
	Knoop hardness, kgf/mm^2	540	530	657	615
Electrical	Surface resistivity, Ω	6×10^9	1×10^9	2×10^{12}	1×10^{19}
	Electric resistivity, Ω•cm	1×10^{12}	1×10^{15}	1×10^{15}	1×10^{18}

The coating material is selected on the basis of its suitability for the specific mask application. For LCD applications, most of the coating materials are emulsion (silver halide based), iron oxide, and chromium.

The advantages of an emulsion mask are low cost, high photosensitivity, good image resolution and contrast, reversal processing, and enhanced image-edge effects [6.1]. The major weak points are relatively high defect levels and a short lifetime. Although the cost of the emulsion coating is low, the total mask cost increases because of the shorter lifetime as compared to hard-surface materials.

Iron oxide has been developed as a see-through mask-coating material and is the second most popular material for hard-surface masking. Its most important characteristic is high transparency in the visible region of the spectrum, making alignment much simpler. Another important optical property is its high transmittance in the red and infrared regions of the spectrum. Iron oxide is very durable and relatively hard, which leads to good scratch resistance, a relatively long working lifetime in production, as well as mechanical resistance to handling with tweezers. The low reflectivity of iron oxide solves the problems of unwanted resist exposure created by reflective mask materials such as chromium. The cross section of a typical iron oxide photomask is shown in Figure 6.1.

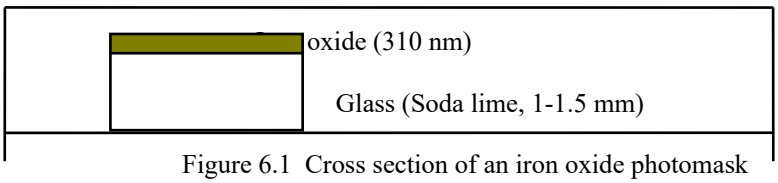

Figure 6.1 Cross section of an iron oxide photomask

Shiny chrome is the most popular hard-surface coating for glass blanks. The most serious problem for the shiny chrome is a high reflectivity, but now is solved by using antireflection layers such as a top coating of chromium oxide. The structures of typical chrome masks are shown in Figure 6.2.

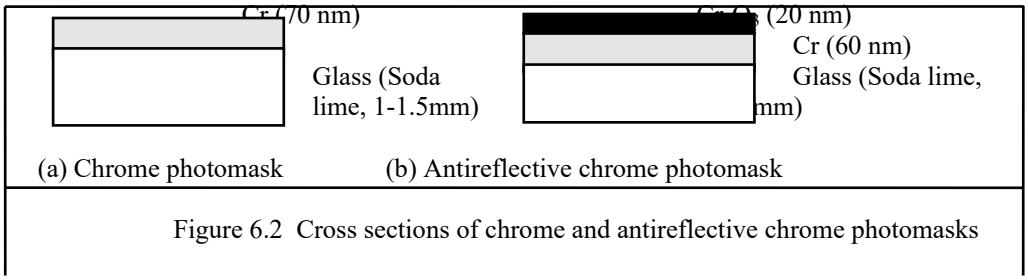

Figure 6.2 Cross sections of chrome and antireflective chrome photomasks

Typically, the linewidth required is 7 - 60 μm depending on the devices. The narrower the linewidth, the denser the patterns can be generated in the LCD devices.

6.2 Micro-Engraving of Photomasks by Nd:YAG Laser

The laser used in this project is a flashlamp-pumped NEC M690B Q-switched CW Nd:YAG laser as described in Chapter 3. The photomasks are the iron oxide photomasks as shown in Figure 6.1.

6.2.1 Calculation of Optical Parameters for Nd:YAG Laser Engraving

Figure 6.3 shows a block diagram of the optical system [6.3]. A HeNe laser is used to align the Nd:YAG laser beam to the surface of a workpiece. The attenuator can continuously reduce the power from the maximum to 2% of the laser output power. The beam expander is used to reduce the far-field divergence angle, and thus to achieve a smaller spot size. The X-Y table is driven by CNC drive motors.

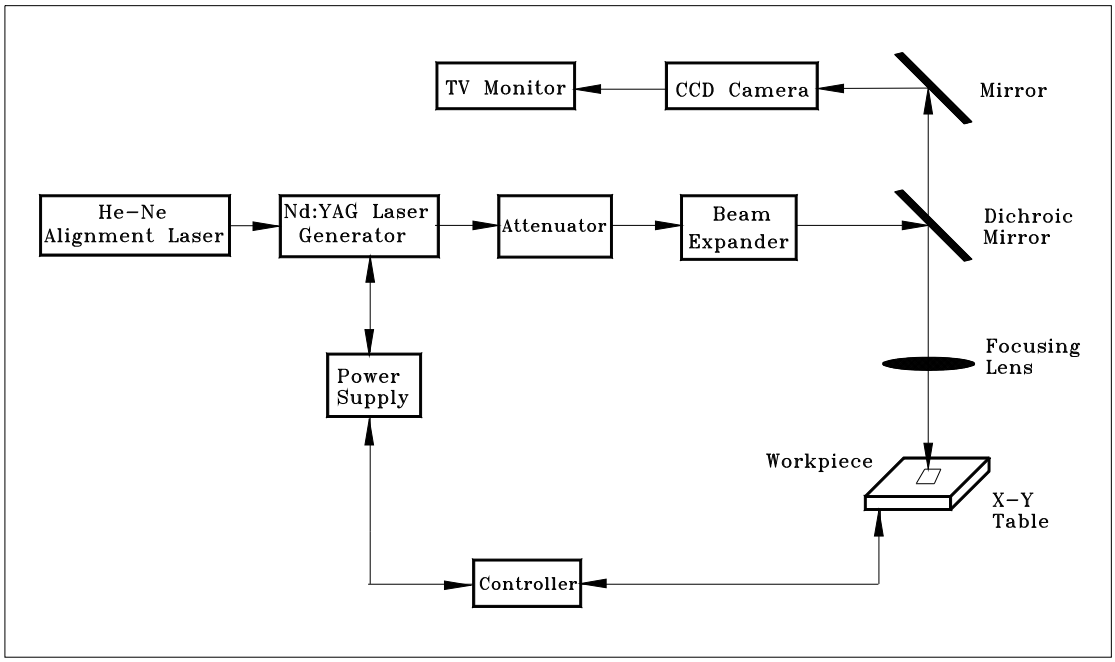

Figure 6.3 Block diagram of optical system with Nd:YAG laser

6.2.1.1 Laser Beam Spot Size inside Laser Resonator

Figure 6.4 shows a schematic diagram of the optical system which includes a laser resonator, a beam expander and a focusing lens. The radii of curvatures for M_1 and M_2 are R_1 and R_2, respectively. The thermal effects of the Nd:YAG rod are represented by a thermal lens with a focal length f_0. M_3 and M_4 are the input lens and the output lens of the beam expander, respectively. M_5 is the focusing lens.

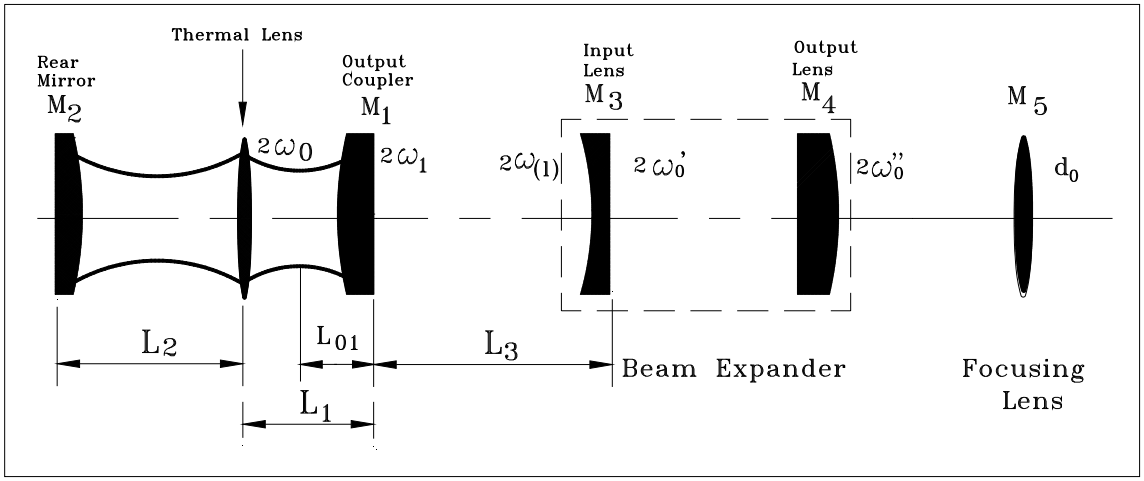

Figure 6.4 Optical diagram of the Nd:YAG laser engraving system

In the resonator, the radius ω_0 of the beam waist and the distance L_{01} between the beam waist and M_1 can be expressed as a function of the equivalent resonator parameters (please refer to section 4.3), i.e.

$$G_1 = 1 - \frac{L_2}{f_0} - \frac{L_0}{R_1} \tag{6.1}$$

$$G_2 = 1 - \frac{L_1}{f_0} - \frac{L_0}{R_2} \tag{6.2}$$

where $$L_0 = L_1 + L_2 - \frac{L_1 L_2}{f_0} \tag{6.3}$$

$$\omega_0^2 = \frac{\lambda L_0 \left[G_1 G_2 \left(1 - G_1 G_2\right) \right]^{\frac{1}{2}}}{\pi \left[G_2 \left(L_0 / R_1 \right)^2 + G_1 \left(1 - G_1 G_2\right) \right]} \tag{6.4}$$

$$L_{01} = \frac{L_0^2 G_2 / R_1}{G_2 \left(L_0 / R_1 \right)^2 + G_1 \left(1 - G_1 G_2\right)} \tag{6.5}$$

$$\omega_1^2 = \frac{\lambda L_0}{\pi} \left[\frac{G_2}{G_1 \left(1 - G_1 G_2\right)} \right]^{\frac{1}{2}} \tag{6.6}$$

and the full divergence angle in the far field, θ, is

$$\theta = \frac{2\lambda}{\pi \omega_0} \tag{6.7}$$

where G_1 and G_2 are the equivalent G parameters and ω_1 is the beam radius on Mirror M_1. Here the laser beam is treated as a fundamental Gaussian beam since an intra-cavity aperture is used inside the resonator.

6.2.1.2 Beam Spot Size after Beam Expander

The most common type of beam expanders is derived from the inverted Galilean telescope which usually has one negative input lens and one positive output lens, as shown in Figure 6.5. The input lens presents a virtual beam focus at the output lens. For low expansion ratios (1.3-20×), the Galilean design is most often employed due to its simplicity, small package size, and low cost [6.4].

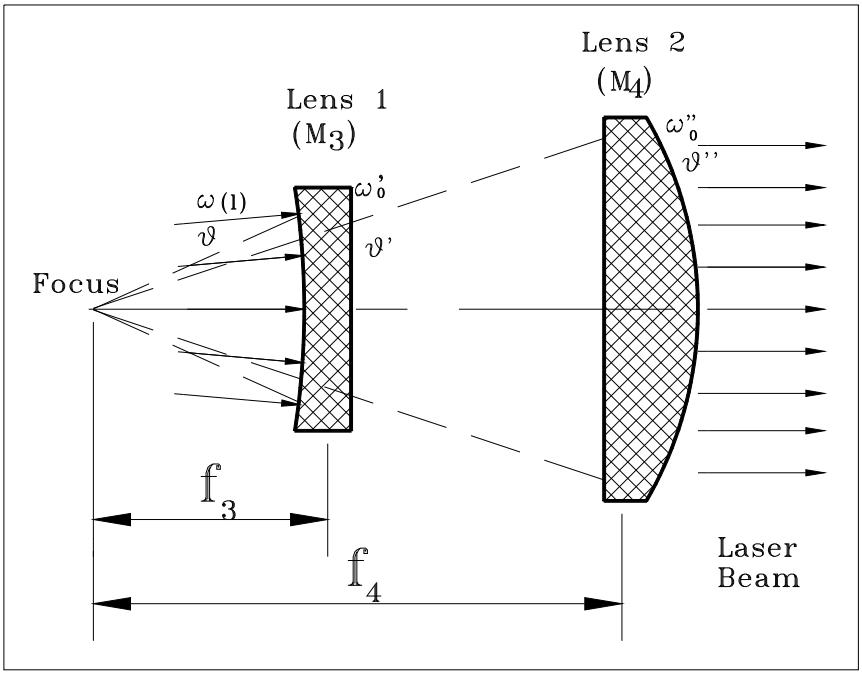

Figure 6.5 The inverted Galilean beam expander

As shown in Figures 6.4 and 6.5, the lens M_3 diverges the laser beam from the laser generator onto M_4. The beam waist ω_0' and divergence angle θ' can be represented by

$$\omega_0' = \frac{f_3 \lambda}{\pi \omega(l)} \tag{6.8}$$

$$\theta' = \frac{2\lambda}{\pi \omega_0'} \tag{6.9}$$

and

$$\omega(l) = \omega_0 \sqrt{1 + \left(\frac{l\lambda}{\pi \omega_0^2} \right)^2} \tag{6.10}$$

where $\omega(l)$ is the radius of the beam entering the lens M_3, f_3 is the focal length of the lens M_3, and l is the distance between the lens M_3 and the beam waist ω_0, which is given by

$$l = L_3 + L_{01} \tag{6.11}$$

Since ω_0' just lies on the focal plane of the lens M_4 with a longer focal length, f_4, the Gaussian beam with a beam waist ω_0' will be collimated by the beam expander. The collimation ratio of the beam expander for a Gaussian beam is as follows [6.5]

$$T = \frac{\theta}{\theta''} = T_1 \sqrt{1 + \left(\frac{l\lambda}{\pi \omega_0^2} \right)^2} \tag{6.12}$$

where T_1 is defined as the beam expansion ratio of the beam expander, which is given by

$$T_1 = \frac{f_4}{f_3} \tag{6.13}$$

The beam size ω_0'' and divergence angle θ'' after the beam expander are given by

$$\omega_0'' = \frac{\lambda}{\pi\omega_0'} f_4 \tag{6.14}$$

and

$$\theta'' = \frac{\theta}{T} \tag{6.15}$$

Substituting Equation (6.8) into Equation (6.14), the following expression can be obtained

$$\omega_0'' = T_1\omega(l) \tag{6.16}$$

From Equations (6.14) - (6.16), it is concluded that the collimation ratio of a beam expander for a Gaussian beam depends not only on the specifications of the beam expander, but also on the laser beam parameters as well as the positions of the optical lenses.

6.2.1.3 Focused Spot Size by Focusing Lens

One of the most important specifications of a focusing lens is the achievable focal spot diameter, which is given by (please refer to section 2.4.2.3) [6.6]

$$d_0 = f\theta'' \tag{6.17}$$

Note that this equation gives an approximation of the focused spot size. It has not taken into account the beam propagation effects, lens aberrations, and ablation thresholds of the coating materials. Substituting Equations (6.7), (6.12) and (6.15) into Equation (6.17), the following expression can be obtained

$$d_0 = \frac{2f\lambda}{\pi T_1\omega_0\sqrt{1+\left(\frac{l\lambda}{\pi\omega_0^2}\right)^2}} \tag{6.18}$$

Therefore, the focal spot diameter can be obtained by knowing the optical system parameters. The set of equations used are (6.1) - (6.5), (6.11), (6.13) and (6.18).

6.2.1.4 Experimental Results and Theoretical Calculations

The experimental results are shown in Table 6.2. The optical parameters used in the theoretical calculations are: $R_1 = R_2 = -0.8$ m, $L_1 = 310$ mm, $L_2 = 360$ mm, $f_0 = 415$ mm at the pumping power of 3.56 kW [please refer to Figure 4.9(a)], and $L_3 = 920$ mm. It is found that the average experimental linewidths come very close to the theoretical values. The discrepancy lies within -8.5% to +2.6% or ±5.22% and can be attributed to the optical aberrations, material interaction, the actual M^2 value, and the depth of focus of the lens.

Table 6.2 Experimental results and theoretical calculations on engraved linewidths

Engraving Speed (m/min)	Pulse Rep. Rate (kHz)	Average Power (W)	Focal Length (mm)	Expansion Ratio (times)	Theoretical Linewidth (μm)	Experimental Linewidth (μm)	Error
1	25	0.15	25	5	8.07	8.0	-0.4%
5.5	5	0.40	50	5	16.14	17.0	+2.6%
5	5	0.50	50	2	40.35	34.0	-8.5%
5	10	0.50	50	3	26.9	26.5	-0.7%

Figure 6.6 shows a photo of two lines engraved with an average power of 0.17 W, a pulse repetition rate of 25 kHz, an engraving speed of 2 m/min and a focal length of 25 mm.

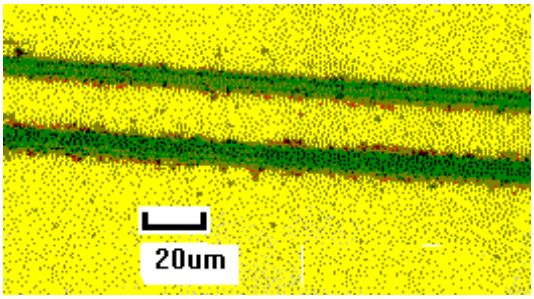

Figure 6.6 Photo of two engraved lines

6.2.2 Parameter Investigation

In this section, the effects of the following parameters on the Nd:YAG laser micro-engraving of photomasks are examined:

- engraving speed
- average laser power
- focus position
- spot overlap

The NEC Nd:YAG laser was employed to carry out the experiments. The experimental set-up is shown in Figures. 3.1 and 6.3. For all the specimen engraved, the required engraving depth of 310 nm is achieved.

6.2.2.1 Effect of Engraving Speed

Figure 6.7 shows the engraved linewidth as a function of engraving speed, where PRR stands for pulse repetition rate. It is obvious that the linewidth decreases with an increase in engraving speed. As the photomask moves faster, there will be less energy absorbed and the line will be narrower.

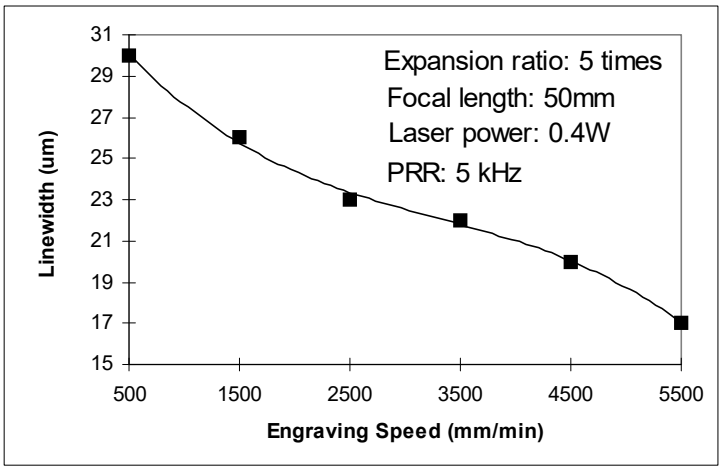

Figure 6.7 Linewidth vs. engraving speed

6.2.2.2 Effect of Average Laser Power

Figure 6.8 shows the variation of the linewidth as a function of average laser power. It is evident that the linewidth increases with an increase in the average laser power due to higher heat input, which produces a wider line.

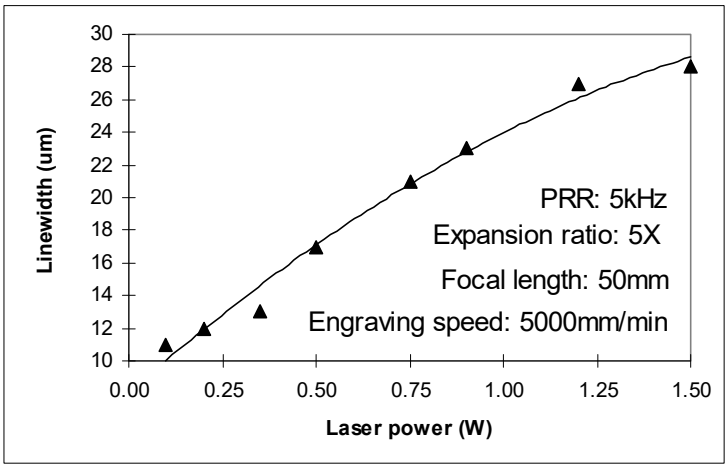

Figure 6.8 Linewidth vs. average laser power

6.2.2.3 Effect of Focus Position

Since the z-axis table is manually adjusted and the pitch of the screw thread is 1 mm, its resolution is rather low. Therefore, the focus position is adjusted using the beam expander in our experiments. This is performed by rotating the input lens of the beam expander to change the lens position (that is the lens M_3 in Figure 6.5). Figure 6.9 shows the linewidth as a function of the scale reading of the lens position. The scale reading of 6 is the focal position. It is clear that the linewidth will increase at defocus positions due to larger spot diameter.

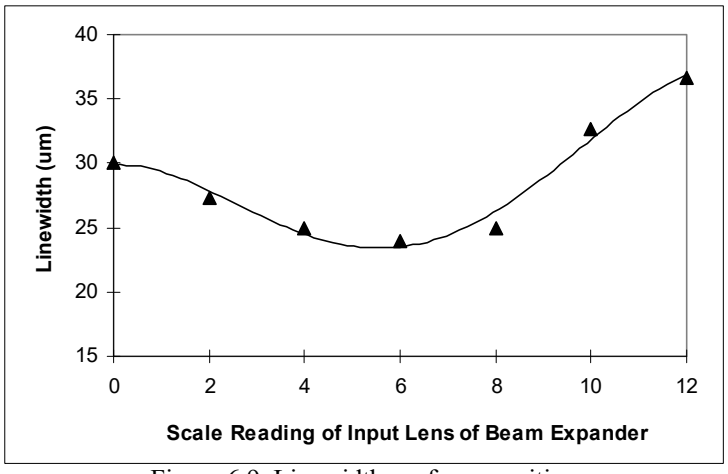

Figure 6.9 Linewidth vs. focus position

6.2.2.4 Effect of Spot Overlap

The pulse repetition rate and the engraving speed together determine the percentage overlap in the laser spots. A good deal of overlap can ensure that the engraving lines are continuous and that spattering will be kept small. If the percentage overlap (in %) is defined as $\mu = x/s$, as shown in Figure 6.10, then [6.7]

$$\mu = \frac{x}{s} = \left(1 - \frac{l'}{s}\right) \times 100\% \qquad (6.19)$$

where s is the spot size, x is overlap length, and l' is the centre-to-centre spacing between the pulsed spots, which is given by

$$l' = \frac{v}{PRR} \qquad (6.20)$$

where PRR is the pulse repetition rate in pps, and v is the engraving speed in m/sec. Qualitatively, in general, $E_{absorbed} \propto \frac{1}{v}$.

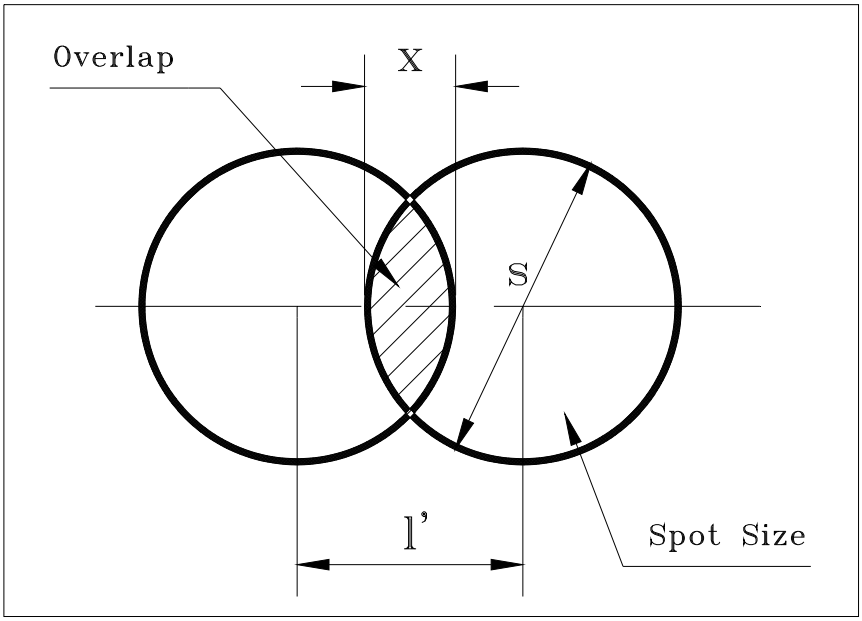

Figure 6.10 Spot overlap

Figure 6.11 shows the linewidth as a function of spot overlap. Here the spot overlaps are changed by changing the engraving speed. It is observed that the linewidth increases with an increase in the spot overlap. In fact, from Equations (6.19) and (6.20), the increase in the spot overlap means a reduction in the engraving speed. Therefore, this result corresponds to those obtained in Figure 6.7.

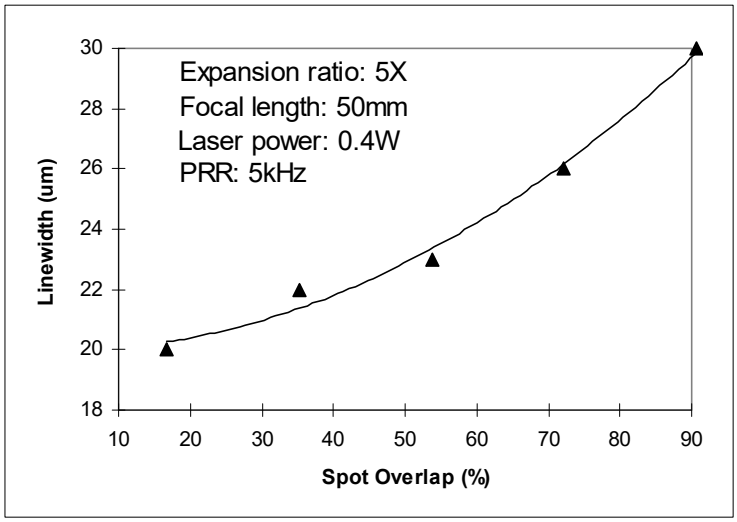

Figure 6.11 Linewidth vs. spot overlap

Figure 6.12 shows the profile of an engraved line obtained using a laser beam profilometer (the diode-laser scanning beam in the profilometer moves along the centre of the engraved line). The line is engraved with a pulse repetition rate of 10 kHz, an engraving speed of 9 m/min, a beam expansion ratio of 5×, and a focal length of 25 mm. The measured centre-to-centre spacing is 15 μm. The calculated spacing from Equation (6.20) is also 15 μm, which is agreeable with the experiments. The overlap from Equation (6.19) (here the measured linewidth is 20 μm) is 35.5%. It is observed that the bottom part of the engraved line is not flat, which is perhaps caused by the gaussian distribution of the laser beam and the re-deposition of molten materials. It is expected that the homogeneous distributions will produce a flatter bottom for the engraving lines.

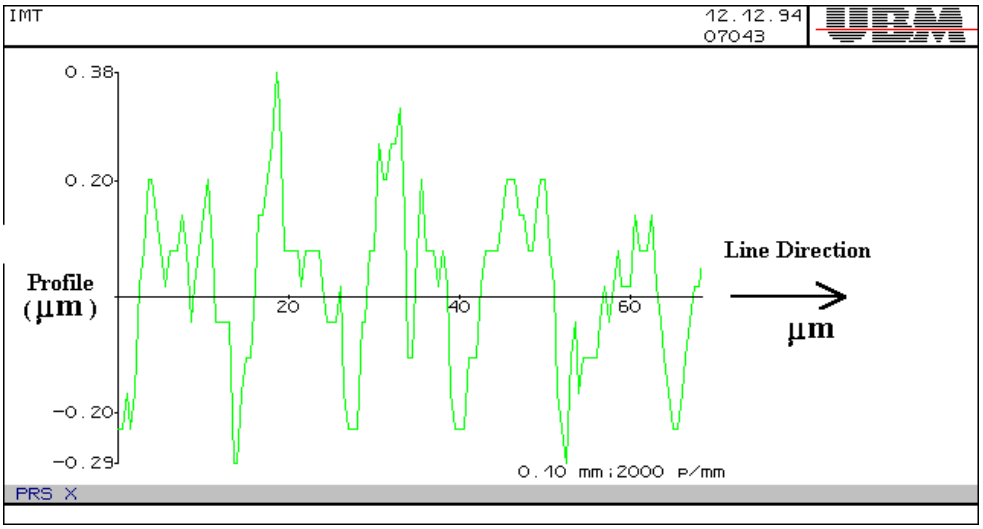

(a) Profile along the direction of an engraved line

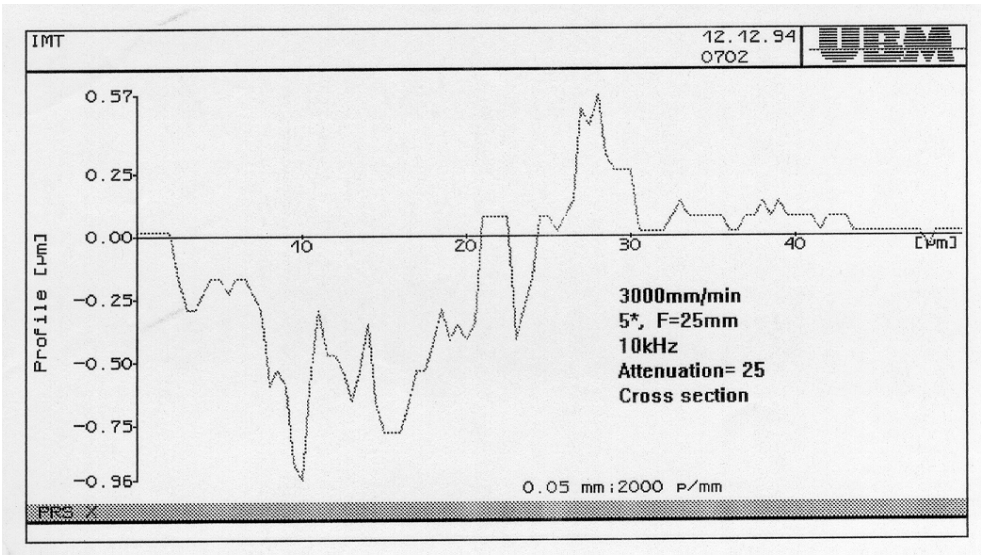

(b) Cross section of the engraved line

Figure 6.12 Profile of an engraved line with the Nd:YAG laser

The following conclusions can be drawn based on the above results and discussions:

1) the higher the engraving speed, the narrower the engraved line;
2) the lower the average power, the narrower the engraving line;
3) the photomask surface should be placed at the focal plane in order to get a narrow line; and
4) a trade-off between the pulse repetition rate and the engraving speed should be performed to obtain a suitable spot overlap.

In general, experimental optimisation of process parameters need to be done in order to obtain a good-quality engraving of photomasks.

6.2.3 Quality of Engraved Lines

The engraved photomask will be used for lithography, which requires the photomask to be transmitting at a given waveband. Therefore, it is important to check the quality of the engraved lines. One method to measure the actual performance is to look at the energy of light transmitted through the engraved lines. Figure 6.13 shows the experimental set-up to measure the transmittance of the engraved lines. For simplicity, a HeNe laser beam is employed. A focusing lens with a focal length of 75 mm is used to focus the laser beam to a small spot size (approximate 15.1 µm). A power meter is used to measure the beam power having gone through the photomask. The photomask moves along the direction perpendicular to the line to be measured.

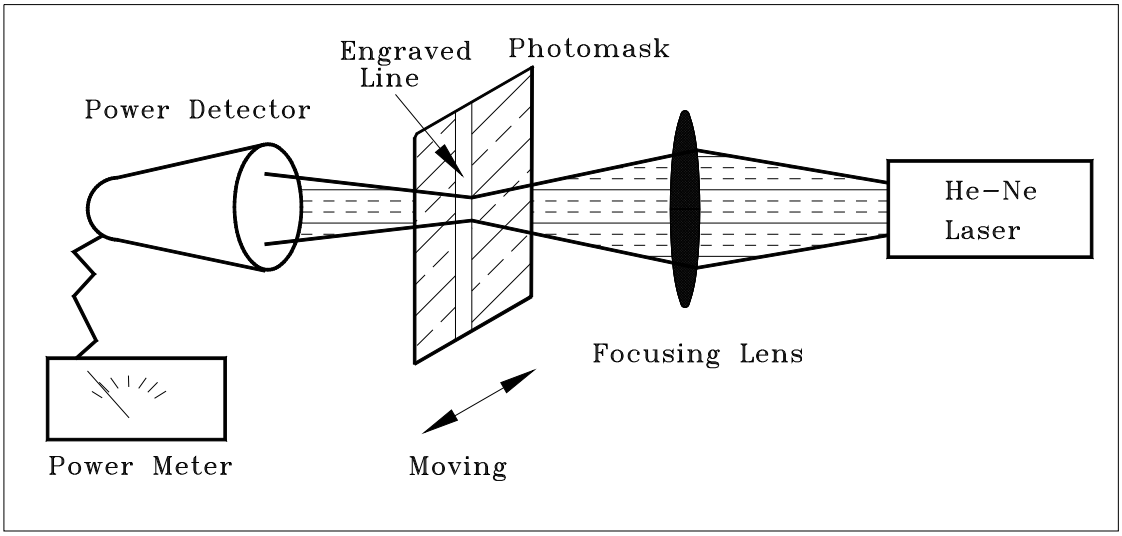

Figure 6.13 Experimental set-up for measuring transmittance of engraved lines

Figure 6.14 shows the transmittance of an engraved line. The transmittance of a line from a standard photomask produced by lithography is also shown for comparison. The linewidths of the two lines measured by an optical microscope are 60 and 35 μm, respectively. It is shown that the distributions of the transmittance curves are similar to one another. This implies that the transmittance performance of the laser engraved line should be reasonably good, too.

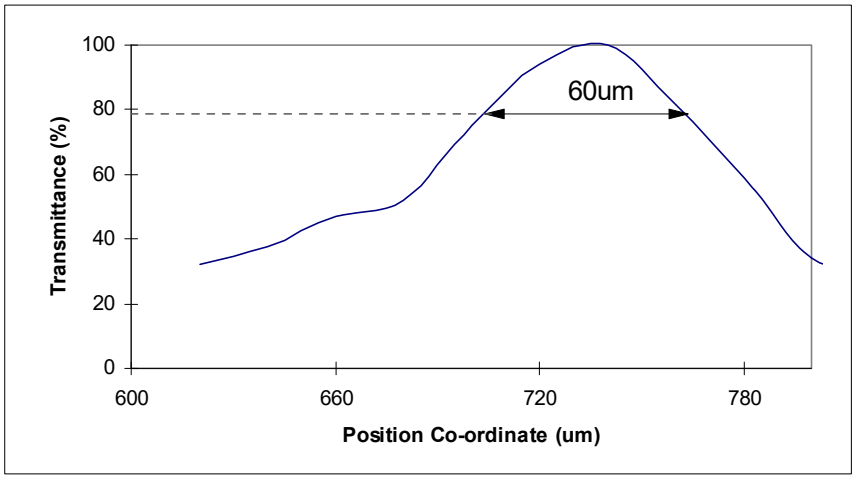

(a) Engraved line by photolithography (The measured line is one of many parallel lines. The distance between two adjacent lines is 626 μm)

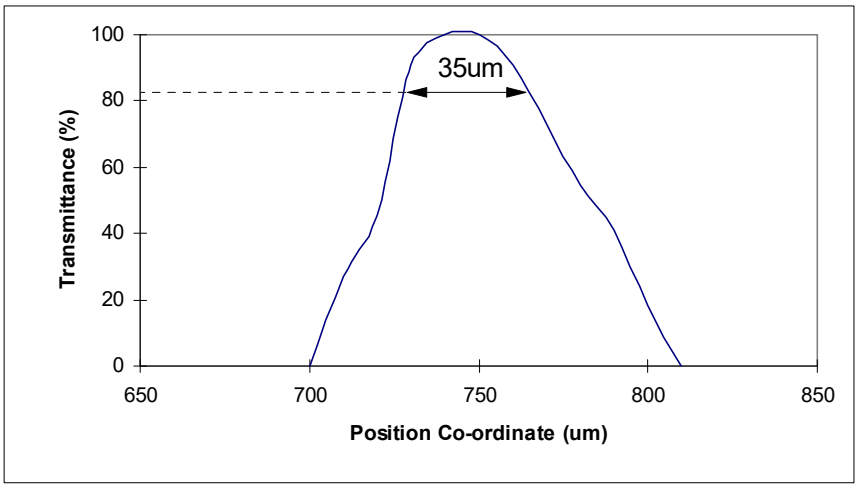

(b) Engraved line by the laser (There is only one line on the photomask)

Figure 6.14 Transmittance of engraved lines

6.3 Micro-Engraving of Photomasks by Excimer Laser

The excimer laser processing system is developed by Exitech Limited, as described in Chapter 3. The block diagram of the system is shown in Figure 6.15. The experiments were done at the wavelength of 248 nm. The photomasks are antireflective chrome photomasks as shown in Figure 6.2(b). The pulse width of the excimer laser is fixed at 20 ns. The peak power or the energy density is changed by changing the pulse energy and the attenuation ratio of the attenuator.

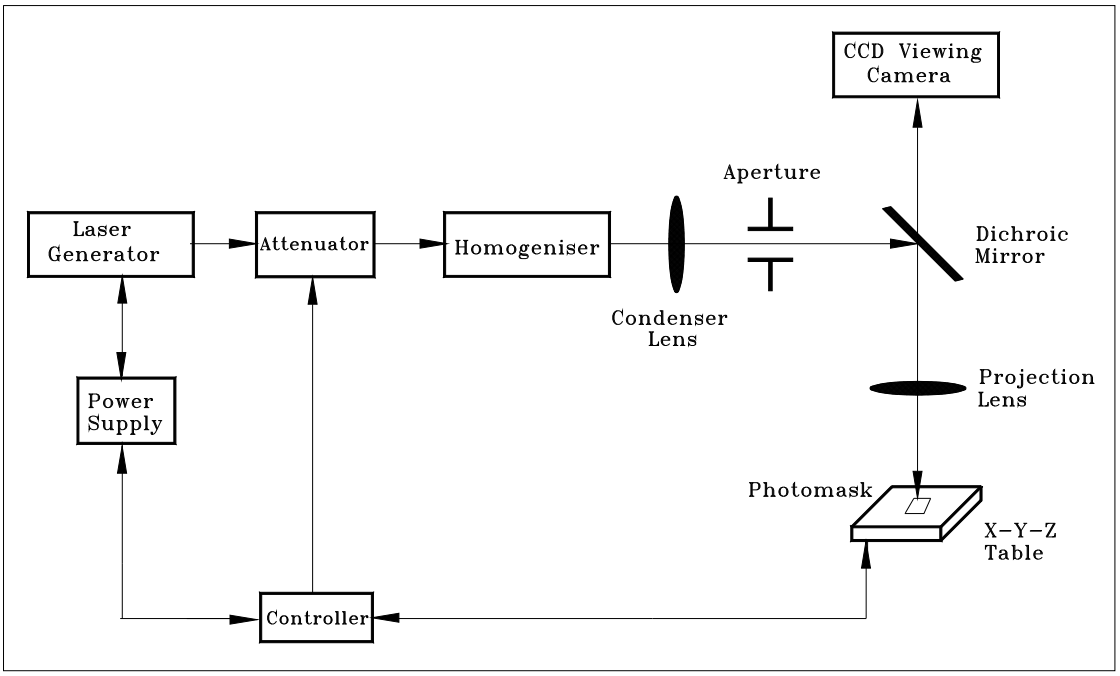

Figure 6.15 Block diagram of the excimer laser processing system

Figure 6.16 shows the engraved rectangular bars at different energy densities, where the aperture is 0.36×3.6 mm, the de-magnification ratio is 36×, the pulse energy is 250 mJ, and the peak power is 12.5 MW. Therefore, the theoretical size of each engraved bar is 10×100 μm. It is observed that the substrates are damaged at energy densities in excess of 4 J/cm^2, and that scribing cannot be performed at energy densities below 1.0 J/cm^2. The density of 2 J/cm^2 gives the best result from these experiments. Furthermore, the engraved linewidth is related to the energy density. Other experiments were done at the pulse energy of 100 mJ and the peak power of 5 MW, as shown in Figure 6.17. The edges of the engraved bars are sharp, and show no heat-affected-zones at suitable energy densities. The results show that an energy density of 1.1 to 2.4 J/cm^2 is suitable for good quality engraving of the photomasks and the optimal energy density is related to the peak power. Rounded edges will occur when the energy density is not strong enough such as 0.9 J/cm^2 (as shown in Figure 6.16). The results are agreeable with the ablation threshold of 1 J/cm^2 for chrome stated in some other literature [6.8].

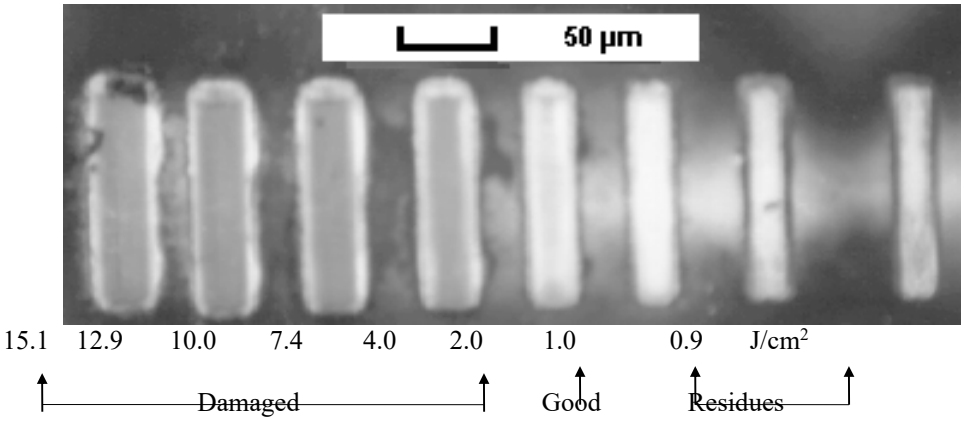

Figure 6.16 Engraved bars at the peak power of 12.5 MW

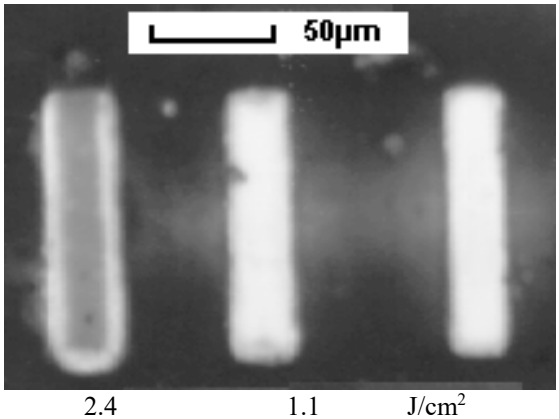

4.3 2.4 1.1 J/cm^2
Damaged Good Better

Figure 6.17 Engraved bars at the peak power of 5 MW

Figure 6.18 shows the effect of overlap on the engraved bars, where the aperture is 0.36×3.6 mm, the de-magnification ratio is 36×, and the pulse repetition rate is 2 Hz. The change of the spot overlap is obtained by changing the moving speed of the engraved masks. The line widths are 10 μm. The spot overlaps are calculated according to Equation (6.19) (here the spot size is 100 μm along the moving direction instead of the diameter). The engraving quality of overlapped areas is the same as that of non-overlapped areas. This means that the overlap can be made as small as possible. Therefore the engraving speed is determined essentially by the length of each bar and the pulse repetition rate.

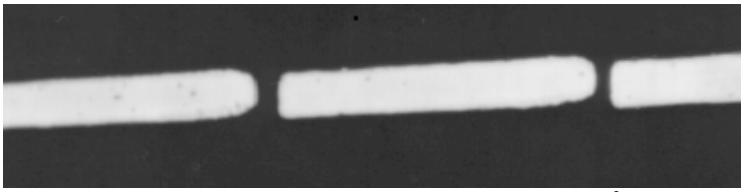

(a) Mask moving: 12.3 mm/min; energy density: 1.4 J/cm^2; no overlap

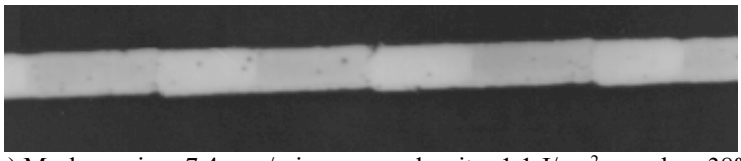

(b) Mask moving: 7.4 mm/min; energy density: 1.1 J/cm^2; overlap: 38%

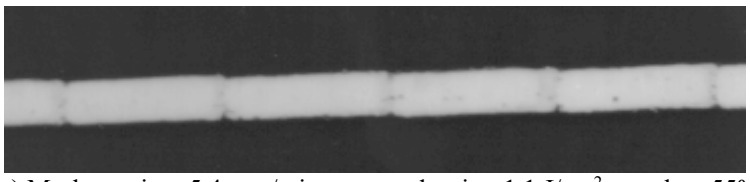

(c) Mask moving: 5.4 mm/min; energy density: 1.1 J/cm^2; overlap: 55%

Figure 6.18 Effect of overlap on engraved lines

Figure 6.19 shows the profile of a line engraved with the excimer laser (the picture is taken with the atomic force microscope). It is observed that the bottom of the line is flatter than that of the line engraved with the Nd:YAG laser as shown in Figure 6.12.

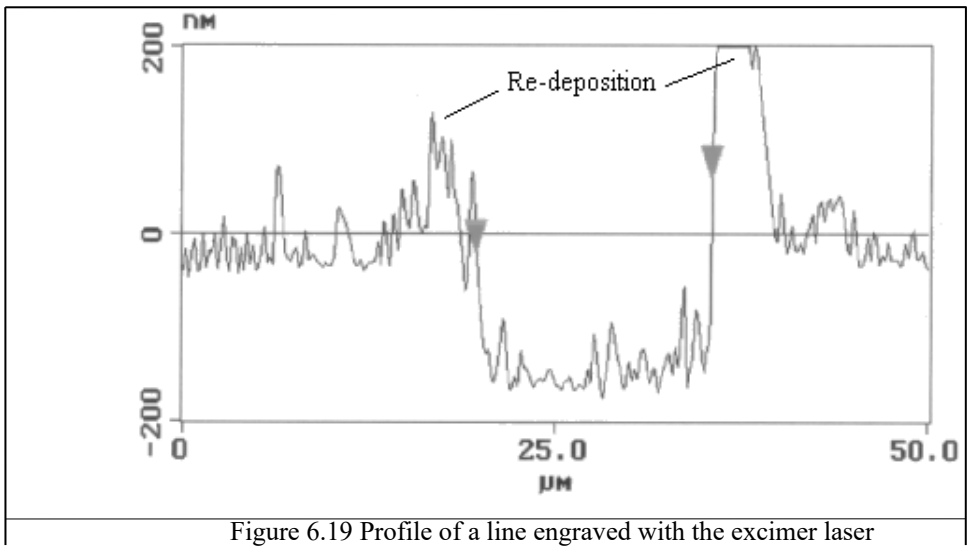

Figure 6.19 Profile of a line engraved with the excimer laser

6.4 Comparison on Laser Engraving of Photomasks

6.4.1 Engraving Speed

The excimer laser operates in a pulsed mode. Its pulse repetition rate is moderate (maximum 200 Hz for the laser used). Therefore its maximum engraving speed is limited by spot overlap and mask imaging size. From Equations (6.19) and (6.20), the engraving speed is given by

$$v = (1 - \mu) \bullet PRR \bullet s \qquad (6.21)$$

For our excimer laser processing system, the maximum imaging size (square) is 1.25 mm (= 5mm/4), and the maximum pulse repetition rate is 200 Hz. Therefore, the theoretical maximum engraving speed can reach 14.25 m/min if the spot overlap is 5%. For a Q-switched Nd:YAG laser, the engraving speed may be comparable but the quality may not be as good. However, in practice, the maximum engraving speed is limited by the table speed of each laser system and optimal combination of process parameters, such as laser power, pulse repetition rate, and percentage of spot overlap.

6.4.2 Engraving Linewidth

In order to achieve the smallest possible spot size, it is useful to expand the laser beam to the diameter of the aperture of the focusing element before focusing. For a high-quality TEM_{00} laser beam, the optical resolution R is approximately given by

$$R = \frac{0.61\lambda}{NA} \qquad (6.22)$$

where NA is the numerical aperture of the objective and λ is the laser wavelength.

Since the wavelength of an excimer laser (248 nm in our case) is only about ¼ that of the Nd:YAG laser (1064 nm), it is theoretically easier to achieve a smaller spot size at the workpiece for the excimer laser than for the Nd:YAG laser. In practice, it is less expensive to find a lens to obtain a line narrower than 10 μm for excimer laser engraving, but difficult to get a lens to produce a line narrower than 10 μm for Nd:YAG laser engraving.

6.4.3 Quality of Engraved Line

The quality of the engraved line for excimer laser processing is much better than that for Nd:YAG laser. Firstly, the heat-affected-zone for excimer laser engraving is very small. The excimer laser beam vaporises the surface layer without disturbing the substrate material and the neighbouring film of the engraved line. Secondly, the lines engraved by excimer laser have sharp edges, as shown in Figure 6.19. This contrasts with Nd:YAG engraving in which scalloped edges are produced [6.9].

6.5 Summary

The Nd:YAG and excimer laser machining systems were used for laser engraving of photomasks. A theoretical expression for calculating focal spot size is derived for the optical delivery system consisting of laser resonator, beam expander, and focusing lens. Measurements on the linewidths agree with the theoretical prediction within -8.5% to +2.6%. Experiments performed on both laser machining systems show that excimer laser engraving of photomasks has many advantages over the use of the Nd:YAG laser. Machining speeds can reach tens of meters per minute, making the technology a viable alternative for LCD patterning and other micro-machining applications such as the laser engraving of ITO coatings. Engraved lines with less than 10 microns of linewidth can be obtained using the excimer laser system with high-quality edges.

6.6 References

6.1 D. J. Elliott, Integrated Circuit Mask Technology, McGraw-Hill Book Company, New York, 1985.
6.2 Shaoguang Microelectronics Company Catalogue, Product Handbook, book 2, Changsha, 1993 (in Chinese).
6.3 Y. H. Chen, W. L. Chen and S. C. Tam, "Calculation of optical parameters in laser engraving of photomasks", Proc. of 1995 International Conference on Optoelectronics and Lasers, Hangzhou (1995), 365-368.
6.4 Melles Griot product catalogue, Optics Guide 5, 1994.
6.5 B. K. Zhou, Y. Z. Gao, J. H. Chen and Z. R. Chen, Principles of Lasers, Tsing Hua University Press, Beijing, 1980 (in Chinese).
6.6 J. James and P. Mike, "Deep hole drilling with lasers", Modern Machine Shop, Vol. 62, No. 1 (1989), 53-63.
6.7 C. J. Monhof, Material Processing with Nd:YAG lasers, Electrochemical Publications Limited, 1988.
6.8 G. A. Shukov and A. Smith, "Micro-machining with excimer lasers", Lasers & Optronics, Vol. 7, No. 9 (1988), 75-77.
6.9 R. T. Crowley, "Laser fabrication of photomasks for hybrid circuits", Proc. of SPIE, Vol. 611 Laser Processing of Semiconductors and Hybrids (1986), 18-22.